RSC Sustainability

Accepted Manuscript

This article can be cited before page numbers have been issued, to do this please use: J. E. Daniel, A. Barnosky, E. Crace and A. Banerjee, *RSC Sustainability*, 2026, DOI: 10.1039/D6SU00221H.

ROYAL SOCIETY OF CHEMISTRY

View Article Online
DOI: 10.1039/D6SU00221H

The CURE described here advances UN Sustainable Development Goals 4, 6, and 10 by blending digital literacy with green nanocatalysis. By integrating LLM-assisted optimization of the synthesis of nano-MFe_2O_4 ($M= Mn^{2+}, Co^{2+}, Ni^{2+}$) and catalytic dye degradation into undergraduate labs, the project modernizes curricula with AI-driven modules (SDG 4). The focus on catalytic wastewater remediation raises awareness of sustainable solutions for global water security (SDG 6). Using a free LLM democratizes high-level research expertise, lowering socioeconomic barriers to STEM entry (SDG 10). Acting as an on-demand virtual teaching assistant, the AI bridges knowledge gaps, offers personalized pacing, and step-by-step breakdowns to accommodate diverse learning needs. To ensure academic integrity, students analyze AI use logs, promoting transparent and ethical prompt engineering practices.

View Article Online
DOI: 10.1039/D6SU00221H

Journal Name

ARTICLE TYPE

Cite this: DOI: 00.0000/xxxxxxxxxx

Leveraging large language models (LLMs) to enhance student inquiry in a nanochemistry teaching laboratory: a Fenton-like oxidation using recyclable ferrite nanoparticle (NP) catalysts.†

Jacob E. Daniel[a], Alex Barnosky[a], Ethan Crace[b], and Abhinandan Banerjee[a,*]

Received Date
Accepted Date

DOI: 00.0000/xxxxxxxxxx

This laboratory module presents a synergistic integration of nanomaterials chemistry and computational literacy by utilizing Large Language Model (LLM) agents as pedagogical partners in the study of transition metal ferrite nanoparticles (NPs). Students investigate the tunable magnetic and electronic properties of spinel-structured MFe_2O_4 (M = Mn, Co, Ni) synthesized using co-precipitation and stabilized with Tween-20. Rather than following a static protocol, students engage in an inquiry-based workflow where LLMs facilitate the optimization of experimental parameters and the interpretation of complex characterization data (spectroscopy, powder X-ray diffraction, electron microscopy, and dynamic light scattering). This partnership extends to the application of these NPs in Fenton-like oxidative catalysis for pollutant degradation, emphasizing both catalytic efficiency and material recyclability. By bridging benchtop experimentation with LLM-guided analysis, the module aligns with UN Sustainable Development Goals 4, 6, and 10, fostering independent scientific inquiry and the digital fluency required for modern, sustainable research. This framework empowers undergraduates to take ownership of their learning, transforming a robust nanomaterials synthesis project into an authentic, AI-augmented research experience.

1 Introduction

As scientific research has become increasingly interdisciplinary, the field of nanoscience is often at the forefront of discovery and innovation.[1,2] Modern nanoscience research is archetypal of an interdisciplinary field, combining elements from traditional fields of study such as chemistry, physics, and engineering with modern disciplines like sustainability and biotechnology[3–5]. Nanomaterials are commonly encountered in various aspects of daily life,[6] including energy generation and storage,[7] healthcare,[8] industrial manufacturing,[9] consumer electronics,[10] and environmental protection.[11] Nanochemistry, the intersection of classical chemistry and modern nanoscience, focuses on the synthesis, characterization, and application of materials on the nanoscale. For emerging scientists, exposure to the principles and techniques of nanochemistry is proving key for career development in the realms of academia, industry, and government policymaking.[12] Providing interested undergraduate chemistry majors with a nanochemistry-specific class furnishes a significant opportunity for those students to develop a comprehensive background in the field of nanoscience.[13,14] Most Canadian and American institutions offering a nanochemistry course to UG students who specialize in chemistry do not provide laboratory experience, relying solely on lecture-based instruction (ESI, Fig S1). However, in our opinion, a lack of laboratory instruction does the students a disservice: passive learning through lectures cannot sufficiently replace hands-on experience with nanomaterials that is essential for comprehension.[15]

Colorado State University (CSU) offers an inquiry-driven and research-based undergraduate level nanochemistry lab course alongside an associated lecture course for upper-level undergraduate chemistry students interested in nanomaterials[15]. While the lecture and the lab courses are not co-requisite, it is recommended that students enrolled in the lecture course also take the lab course to experience practical application of the content

[a] Department of Chemistry, Colorado State University, Centre Mall, Fort Collins, CO, USA; Tel: 1 970 491 2130; E-mail: abhinandan.banerjee@colostate.edu
[b] Analytical Resources Core, Colorado State University, 1301 Centre Ave Mall, Fort Collins, CO 80523-1872, USA

† Supplementary Information available: [(1) Nanochemistry course offerings in Canadian and United States universities; (2) detailed experimental workflow; (3) sample pre-lab questions; (4) instructions to students for the synthesis of MMFNPs; (5) procedure for the catalytic degradation of methylene blue; (6) instructions for determining the band gap using the Tauc plot method; (7) PXRD patterns for all of the MFe_2O_4/Tween-20 NP explanation of amorphous structure for $NiFe_2O_4$; (8) additional collected DLS characterization data; (9) integration of ethical LLM usage within the CURE; (10) questions for LLM-guided active inquiry; (11) Sustainability spotlight]. See DOI: 00.0000/00000000.

View Article Online
DOI: 10.1039/D6SU00221H

taught in lecture, and *vice versa*. Since this course is focused on experimental synthesis and data analysis, collaboration with the Analytical Resources Core (ARC), a shared instrumentation facility at CSU, is utilized to provide students with access to XRD and scanning electron microscopy (SEM), while optical spectroscopy can be performed with relatively inexpensive Vernier spectrofluorometric instruments. Although many of these characterization methods require specialized software interfaces, widely available analysis tools like OriginLab^{TM}, FiJi/ImageJ, and Mercury® are either freeware or offer extended free trials for actively enrolled students. Finally, our experiments utilize low-cost and nontoxic chemicals that are "friendlier" to an undergraduate student compared to other pedagogical exercises such as the synthesis of CdSe quantum dots[16,17], and may be procured from a general vendor through online shopping platforms such as Amazon.

Inquiry-driven and research-based course design, such as the course-based undergraduate research experience (CURE) model, has been extensively reported in the literature to enhance the undergraduate student experience, promote academic achievement, and provide opportunities for career development.[18–20] A CURE-based course allows students to test their own hypotheses and design their own experimental setup, promoting student retention and addressing inequalities that are inherent in traditional undergraduate research programs.[21] Browsing the literature reveals that there are a growing number of chemistry CUREs available; however, they are mainly concentrated in the biochemical and organic chemistry disciplines or associated with "general chemistry" modules.[20,22,23] To maximize student involvement and interest, CUREs should address subject matter that students can connect to visible problems in modern society, such as the need for sustainably sourced materials in the fields of healthcare, energy generation, environmental remediation, and optoelectronic applications. More recently, sustainable and green synthetic methods have been applied to the field of materials chemistry, particularly to functional nanomaterials synthesis.[24,25] These efforts include not only reducing the amount of toxic precursors, capping agents, or reducing agents, but also increasing energy efficiency and limiting costs.[26,27] Therefore, the first experiment in the CURE-based nanochemistry lab course at CSU was based on a low-energy, environmentally friendly co-deposition synthesis of magnetic spinel mixed-metal ferrite nanoparticles (MMFNPs) of the generic formula MFe_2O_4 (M = Mn, Ni, Co) capped with polyoxyethylene (20) sorbitan monolaurate (Tween-20), a common nontoxic surfactant used in multiple personal care products.

Transition metal oxide nanoparticles are widely studied for a variety of applications, as demonstrated by the multitude of review articles present in the literature.[28–30] Of the iron oxide family, magnetite nanoparticles (Fe_3O_4) are the most widely studied.[31] However, doping of a different divalent metal cation into the magnetite unit cell produces mixed-metal ferrite compounds (MFe_2O_4; M = Mn, Ni, Co). Actively pursued for applications in biomedicine, electronics, energy, and bioremediation, these nanomaterials exhibit diverse optical, electronic, and magnetic properties depending on their size and composition.[30,31] In particular, Banerjee *et al.* have published a comparative study of the magnetic properties and relaxometric parameters for poly(ethylene glycol) coated spinel ferrite NPs with potential applications as T_2 MRI contrast agents[32]. Furthermore, the MMFNPs can be consistently synthesized (albeit with a low level of size and shape control) by a facile and sustainable co-deposition process.[33,34] As a result, this family of iron oxide based nanomaterials is perfect for the CURE environment, coupling a beginner-friendly synthesis protocol with broad instrumental characterization, and simple chemical tunability leading to identifiable impacts on material properties. The broad goal of this experiment was to introduce students to a flexible and widely used nanomaterial synthetic technique while training them to operate and/or understand common characterization methods, using compounds that they personally synthesized – a key to increasing student interest and engagement.[15] Table 1 briefly highlights key material properties that were explored, the characterization technique and associated software employed to analyze each property; this created a trove of diverse data for the students to practice their data collection, analysis, and processing skills on.

The integration of LLMs into CUREs and teaching laboratories marks a transformative shift toward AI-augmented inquiry, aligning with the pedagogical requirements of modern, sustainable science education[35]. By serving as an interactive interface between complex theoretical frameworks and benchtop experimentation, LLMs empower students to navigate the iterative nature of materials synthesis (in our case, the green production of transition metal ferrites) while fostering critical thinking and digital literacy[36].

Relevant literature increasingly supports this "human-in-the-loop" model; for instance, researchers have demonstrated that LLMs can function effectively as personalized tutors for troubleshooting experimental design, while other studies highlight their efficacy in helping students synthesize vast datasets, such as relating spectroscopic characterization to catalytic performance[37–39].

Furthermore, allowing the use of AI resources or implementing LLM training into an educational program can lower barriers to entry for students with less developed skill sets and promote active learning; for example, in disciplines requiring programming backgrounds such as physical or computational chemistry[40].

Prompting students to use AI to optimize reaction conditions (for instance, minimizing reagent waste or shifting towards greener solvent systems) is another avenue, helping instructors directly embed the principles of green chemistry and sustainability into the laboratory workflow[41,42].

In the last year, a growing number of chemical educators have realized this potential, developing undergraduate lab procedures for AI-assisted syntheses of organic molecules, metal-organic cages, and SiO_2 nanoparticles, showcasing a variety of laboratory subjects that benefit from the framework provided by thoughtful proper LLM inclusion[43,44].

This technological scaffolding not only lowers the barrier to authentic research, but also prepares UGs for the evolving demands of interdisciplinary fields where AI-driven data interpretation is becoming a standard laboratory competency, thereby directly advancing the pedagogical goals outlined in the United Nations Sustainable Development Goals. On that note, this 'mini-

View Article Online
DOI: 10.1039/D6SU00221H

Table 1 Data processing and analysis techniques associated with this experiment

Nanomaterial property	Measurement technique	Data processing skill (Software)
Band gap	UV-Vis spectroscopy	Tauc plot (OriginLab®)
Hydrodynamic radius	Dynamic light scattering	Data extraction and plotting (OriginLab®)
Size and morphology	Scanning electron microscopy	Size evaluation and distribution profile (FiJi)
Phase identification	Powder X-ray Diffraction	Phase matching (CrystalDiffract®, Mercury®, COD)
Surface functionality identification	IR spectroscopy	Peak picking and assignments (OriginLab ^{TM})

project' aligns with UN SDG numbers 4 (providing quality education and hands-on laboratory training, including ethical LLM usage, to our future scientists-in-training) and 6 (ensuring availability and sustainable management of water and sanitation through effective wastewater remediation): key sustainability targets in today's world.

2 Materials and methods

2.1 Student cohort

The students enrolled in this laboratory course were juniors and seniors (third- and fourth-year students) majoring in chemistry at Colorado State University. The majority were co-enrolled in a lecture module, also dealing with chemistry at the nanoscale. The pre-requisites for this laboratory module included successful completion of the introductory inorganic chemistry lecture and laboratory components. The students had already received laboratory safety training (including the study of material safety data sheets - MSDS - for hazard warnings). Under the supervision of the graduate teaching assistant (JED), the students worked individually over the course of five 3.5 h laboratory sessions, meeting once a week. A total of five students participated in this course; we anticipate that an enquiry-driven learning project like the one described here is best optimized for a comparable class size. The experiment was planned as an introduction to typical research practices in inorganic nanochemistry incorporating a central question: "what role is played by MFe_2O_4/Tween-20 NP in the catalytic oxidative degradation of methylene blue as a sample contaminant in a wastewater matrix?" As an exercise in enquiry-based learning, this project tasked students with finding the answers to a series of scientific questions every week. Simultaneously, they gained valuable experience in the use of a series of instruments typically used in nanochemistry research laboratories for characterization of nanoscaled materials.

2.2 Learning objectives

The following experimental learning objectives were identified:

1. Stoichiometric synthesis of MFe_2O_4/Tween-20 NP using co-precipitation under an inert atmosphere.

2. Hands-on experience with typical operations performed during inorganic nanomaterial separation, isolation, and sampling: centrifugation, magnetic separation, drop-casting, decantation, aspiration, and others.

3. Student-led collection of UV-visible and IR spectroscopy including data interpretation through comparison with literature examples.

4. Student-led use of a DLS instrument for NP size and surface charge determination.

5. Data processing and interpretation for assessing the characteristics of the synthesized nanoparticles: PXRD and SEM.

6. Following the trajectory of a NP-catalyzed reaction (decoloration of methylene blue in water) using spectrophotometry.

7. Developing data visualization and scientific communication skills.

For the techniques where we were unable to let the students use the instruments independently (SEM and PXRD) the class was given an opportunity to watch the instrument at work, including steps such as sample loading and/or imaging. For UV-Vis, IR, and DLS, the students were instructed in the principles behind the technique, and performed the protocol themselves while closely monitored by JED.

The LLM-specific learning objectives were identified as the following:

1. Students must demonstrate the ability to construct targeted prompts using chemical principles (*e.g.*, lattice energy, oxidation states) to predict experimental outcomes, successfully distinguishing between valid scientific reasoning and "hallucinated" AI responses.

2. After collecting raw characterization data (*e.g.*, XRD, UV-Vis), students are expected to use LLMs to perform preliminary calculations, subsequently verifying these results against manual calculations to evaluate the accuracy and limitations of AI-assisted data analysis.

3. Students should be able to identify specific steps where reagent toxicity or energy consumption can be minimized with the help of LLMs, thereby directly addressing SDG 6.

4. Students will be trained in the creation and curation of an "AI-Integration Log" that critiques the utility of the LLM in their research workflow, identifying cases where the AI failed to provide accurate guidance and explaining the chemical principles that corrected the AIś error.

View Article Online
DOI: 10.1039/D6SU00221H

2.3 Materials

All chemicals were already present in the inorganic chemistry teaching laboratory stock and were used without further purification. Iron (III) chloride hexahydrate ($FeCl_3 \cdot 6H_2O$) was originally sourced from Mallinkrodt. Manganese (II) chloride dihydrate ($MnCl_2 \cdot 2H_2O$) was obtained from Sigma-Aldrich. Cobalt (II) chloride hexahydrate ($CoCl_2 \cdot 6H_2O$) and nickel (II) chloride hexahydrate ($NiCl_2 \cdot 6H_2O$) were obtained from Alfa Aesar. Sodium hydroxide (NaOH) was obtained from Fisher. Tween-20 was obtained from Hznxolrc (ordered using Amazon). DI water was used throughout the experiment. Nitrogen gas (technical grade) was purchased from AirGas. Methylene blue powder was obtained from HiMedia (Amazon, HiMedia GRM956-100G Methylene Blue). Hydrogen peroxide (30% w/w) was purchased from Millipore Sigma and stored at 4°C.

2.4 Synthesis of the MMFNPs

Step-by-step instructions for the synthesis as supplied to the students may be found in the ESI. The students prepared the precursor solutions of the divalent metal salt (10 ml, 0.25 M) and iron (III) chloride hexahydrate (10 ml, 0.5 M). These were subsequently heated to *ca.* 60°C. A gently boiling aqueous solution of NaOH (120 ml, 0.7 M) was kept under a nitrogen gas flow. To this, students added approximately 0.1 mL Tween-20 to prepare a *ca.* 1 mM solution. A reflux condenser was fitted, completing the set-up as shown in Figure 1. The students then injected both precursor solutions simultaneously into the alkaline reaction medium; this can be done by two individuals synchronously, or by a single person using a two-handed injection approach. The solution was refluxed under nitrogen flow for 1 h. After 1 h, the refluxing was discontinued, and the reaction mixture was cooled to room temperature. The MFe_2O_4 NPs were recovered by centrifugation (FisherBrand, AccuSpinMax, 10,000 rpm) and washed twice with DI water containing 5 wt % Tween-20. Finally, the NPs were left to dry under air.

2.5 Sample preparation for characterization techniques.

The students were encouraged to observe and participate in sample preparation for the various characterization techniques. The students themselves prepared the samples for UV-visible spectroscopy, IR spectroscopy, DLS, and SEM. For PXRD, students observed sample preparation as performed by the GTA.

2.5.1 UV-Visible spectroscopy.

For recording the optical spectra of the precursor and the final products were diluted with DI water in a quartz cuvette, and then placed in a Vernier GoDirect spectrophotometer. DI water was used as the background. Approximately 0.1 mL of the post-centrifuge NP slurry (*ca.* 20 mg) was added to 30 mL of DI water, sonicated for 15 min, and 1 mL of this was added to a quartz cuvette containing 2.5 mL of DI water, thoroughly mixed, and the spectrum was recorded. The students were given instructions on the conversion of the UV-Vis data for MMFNPs to representative Tauc plots for the estimation of the band-gap of MFe_2O_4/Tween-20 NP (ESI).

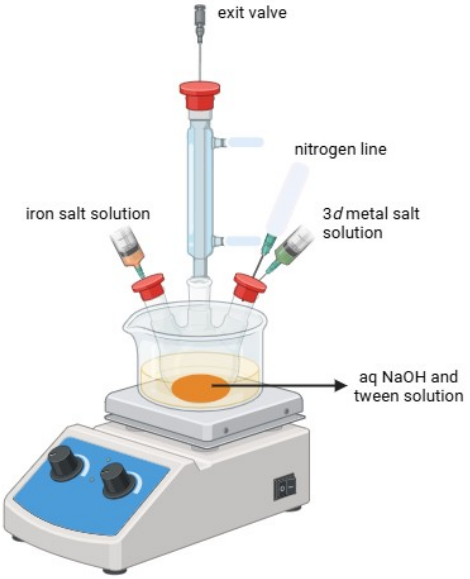

Fig. 1 Experimental set-up for the synthesis of MFe_2O_4/Tween-20 NP by students.

2.5.2 ATR-IR spectroscopy.

The students recorded ATR-IR spectra for Tween-20 and MFe_2O_4/Tween-20 NP on a Nicolet Summit portable IR system. The number of scans per sample was fixed at 32, and the resolution was set at 8 cm^{-1}. The students were encouraged to replot their data and identify/highlight chemically relevant peaks for each sample.

2.5.3 Dynamic light scattering.

In order to determine the average dimensions of the MMFNPs, dynamic light scattering (DLS), also known as photon correlation spectroscopy, was applied. This technique measured hydrodynamic diameters of the MFe_2O_4/Tween-20 NP, as well as the polydispersity index (PDI). Diluted samples of the as-synthesized NP dispersion (50- to 100-fold dilutions) were used to avoid multiple scattering, and the samples were sonicated in a commercial ultrasonic bath (US Solid) for 10 minutes prior to measurements. Aggregates were eliminated by filtration through a 0.22 μm PTFE syringe filter. The measurements were conducted using the Be-Nano 180 Zeta Max (Bettersize) and the particle dimensions were calculated from the autocorrelation function of the intensity of light scattered from the particles. Disposable poly(styrene) cuvettes were used for sample measurements.

The rate of droplet movement under the influence of an external oscillating electrical field with a voltage of 150 V (electrophoretic mobility) was also measured with the same instrument, in folded capillary cells obtained from Bettersize. The measured electrophoretic mobilities were converted to ζ-potentials by the instrument software using Henry's equation:

$$U_e = \frac{2\varepsilon\zeta}{3\eta} \cdot f_{a\kappa} \quad (1)$$

where U_e is the electrophoretic mobility, ε is the dielectric con-

View Article Online
DOI: 10.1039/D6SU00221H

stant, ζ is the zeta potential, η is the viscosity of the dispersant, and $f_{a\kappa}$ is the Henry function. The Smoluchowski approximation, $f_{a\kappa} = 1.5$, was used for high ionic strength media, given that water was the bulk phase in all the measured systems. Note that the DLS measurements were performed by the students themselves with some guidance from JED, who had previously received extensive training on the instrument.

2.5.4 Scanning electron microscopy.

Post-centrifugation MFe_2O_4/Tween-20 NP slurry was diluted tenfold in water, and sonicated in a commercial ultrasonic bath (US Solid) for 10 minutes. 50 μL of the diluted MFe_2O_4/Tween-20 NP sample was drop-cast directly on a SEM sample stub, and allowed to dry for a week. The following week, a two-hour session was dedicated to examining the student samples under a JEOL JSM-IT800(HL) field emission SEM and recording micrographs. This part of the experiment was performed by ARB, with the students and JED present in the room for the duration of the experiment. The students were previously trained on extracting average particle sizes and particle size distributions from the images using FiJi. Image colouring using an LLM image processing website *(https://imagecolorizer.com/colorize)* was added as an at-home activity, which the students responded favorably to.

2.5.5 Powder X-ray diffraction.

For the preparation of PXRD samples, two avenues were explored: (1) a slurry of the MFe_2O_4/Tween-20 NP sample was drop-cast on a silicon zero background holder and allowed to dry overnight; or, (2) a fine powder was sprinkled onto Dow Corning high vacuum grease or commercial petroleum jelly coating a silicon zero background holder. The grease typically contributes very weak signals (representative of amorphous materials) in the data, and a weak diffraction peak at about 22° in the case of petroleum jelly. The sample was then handed over to the XRD scientist (EC) at CSU's ARC, who recorded a diffractogram of the sample on a Bruker D8 Discover with DaVinci. All experiments were performed with a copper (Cu) K_α X-ray source, divergent beam optics with a 0.6 mm slit and 2.5° Soller slit, FLIPSTICK sample changer, anti-scatter blade, 2.5° Soller slit on the diffracted optics, and a Lynxeye XE-T detector in 1D mode. All data were collected as symmetric θ-2θ scans in the range of 10-120° 2θ with 0.02° steps and integration time of either 0.5 or 0.8 seconds per step (approximately a 46 or 74 minute scan, respectively). Samples were spun continuously during data collection.

Data were collected over a period of time where a X-ray tube change was required due to the aging X-ray tube producing tungsten (W) L X-ray wavelengths in addition to the typical Cu $K_{\alpha1}$, $K_{\alpha2}$, and K_β wavelengths. Scans collected before the tube change included a 0.02 mm nickel filter before the Soller slit in the diffracted beam path to eliminate any diffraction caused by W X-rays. The nickel filter caused a 50% decrease in Cu Kα x-ray wavelengths' intensity, requiring the longer scan times mentioned above. Shorter scan times without the nickel filter were used after the tube change.

The data were communicated directly to the students, who were instructed to plot a diffractogram from the experimental data in the program CrystalDiffact®.[45] The students were also trained on obtaining crystallographic information files (CIF), with the file extension *.cif*, for some of the probable phases - for $MnFe_2O_4$, for instance, the experimental diffractogram was compared to the powder patterns for $MnFe_2O_4$, MnO, and magnetite. The standard powder patterns were obtained from the crystallographic open database (COD).[46–54] The students then opened the *cif* files using Mercury®,[55] a free crystal structure visualization tool developed by the Cambridge Crystallographic Data Centre. The students obtained the powder diffraction pattern for each 'standard' phase of interest, and plotted the relevant diffractograms directly under the experimental diffractogram for phase identification through visual inspection.

2.6 MFe_2O_4/Tween-20 NP catalyzed degradation of methylene blue in simulated wastewater.

6 mL H_2O_2 was added to 95 mL of 16 μM methylene blue solution and stirred briefly. The pH was raised to 11 by the dropwise addition of 2 M NaOH. The sample was stirred magnetically for five minutes, then an initial UV-Vis sample was taken. Approximately 25 mg of the MMFNPs were added, and the mixture was agitated rapidly with a glass rod for 30 seconds. The reaction was then allowed to progress to completion under UV illumination with magnetic stirring set to 100 rpm. A 1 mL aliquot withdrawn every 10 minutes until a total of 60 minutes had passed. Every aliquot was diluted with 1 mL H_2O before analysis. Following the completion of the reaction, the stir bar was utilized to magnetically recover the nanoparticles, and transferred to a new beaker for the second and third catalytic cycles, respectively. A copy of the student procedure handout is available in the ESI.

2.7 LLM incorporation within pedagogy.

The LLM used in this CURE was Google Gemini 2.5 Flash, accessed over several weeks in the fall of 2025. The mode of pedagogical usage of the LLM has been described (*vide infra*). All prompts were designed initially by the students, and curated by JED and AB to ensure pedagogical alignment with the CURE objectives. Crucially, all LLM-generated outputs, including hypotheses, calculations, and interpretations, were critically reviewed, verified, and validated first by the students, and then by the authors of this publication, against primary scientific literature and empirical laboratory results. We note that no LLMs were used to generate original experimental data.

3 Results and discussions

3.1 Workflow

Weekly pre-lab lectures were given at the discretion of the course instructor and TA, covering abridged theoretical background as well as practical demonstrations of data collection and analysis. However, it is to be noted here that the 'discussion' for each characterization technique should be driven by the students in consultation with the TA. Additionally, students should already be proficient in (or be given instructions on) using a scientific search engine such as SciFinder or Google Scholar to access publications that have previously characterized MMFNPs. They should then

View Article Online
DOI: 10.1039/D6SU00221H

extract the relevant results from these reports and compare those with the data they have recorded in class (Table 2). This comparison was assigned as weekly continuing 'at home' assignments for the duration of the project, and eventually culminated in a submitted lab report using a communication template.

Table 2 Homework assignments associated with this project

Week number	Homework assignments
1	N/A (NP synthesis) literature study
2	UV-Vis data plotting Tauc plot and band-gap determination
3	DLS data plotting IR data plotting, peak assignment, literature comparison
4	Particle size distribution from SEM PXRD data plotting, phase identification
5	Kinetics of MFe_2O_4 catalyzed methylene blue degradation Catalytic data processing
6 *	Report in communication format.

3.2 Electronic properties: UV-visible spectra and Tauc plot

In Figure 2, we show the UV-visible spectra of the metal precursors in acidic solutions, as well as that of the MFe_2O_4/Tween-20 NP [Figure 2(b-d)]. The *d-d* or ligand to metal charge transfer (LMCT) bands are typically expected from solutions of 3*d* metal salts; for instance, the mixed iron chlorides dissolved in 2(M) HCl show a single peak around 300 nm, typically associated in the literature with various $[FeCl_x]^{y+}$ species. These bands were absent in the MFe_2O_4/Tween-20 NP samples; instead, a shoulder appeared at lower wavelengths, corresponding to high-energy electronic transitions associated with ferrite NPs, indicating conversion of the metal chlorides to MMFNPs[56].

The students converted the UV-visible spectrum of the MFe_2O_4/Tween-20 NP to a Tauc plot by using the Tauc equation, represented below. This plot is used extensively for easy determination of the approximate optical band-gap of semiconductors through simple extrapolation. Details for the calculations may be found in our previous report[15], as well as the ESI.

$$(\alpha h\nu)^n = K(h\nu - E_g) \quad (2)$$

The band gap energy of MFe_2O_4/Tween-20 NP is determined from the Tauc plot, wherein $(\alpha h\nu)^n$ is plotted as a function of $h\nu$, followed by taking the extrapolation in the linear area across the energy axis in the corresponding graph [Figure 2(a)]. The values obtained by the students for the different MFe_2O_4 NPs were deemed to be within acceptable ranges after they obtained 'expected values' for these band gaps from a literature search.[57–60] This also provided the instructors with an opportunity to discuss some of the finer points associated with a simple Tauc plot. Namely, despite widespread use owing to its simplicity, it has several drawbacks, and many complex modifications have been suggested for more accurate determination of the optical band-gap of NPs from their spectroscopic data[61].

3.3 Surface properties: IR spectroscopy and surface zeta potential measurement.

IR spectroscopy plays a vital role in determining the surface composition of nanoparticulate matter, which in turn has a profound effect on their functional properties, such as solubility and catalytic behaviour[62]. Students utilized IR spectroscopy (and zeta potential analysis, discussed later) to characterize the nanoparticle surface. During the synthesis of the MMFNPs, students added Tween-20 to act as a surfactant, terminating NP growth and increasing colloidal stability of the ferrite NPs in aqueous solution. As a result, students should observe Tween-20 signatures in the nanoparticle IR spectra. Figure 3 displays a representative IR spectrum of Tween-20 covered MMFNPs (sample), with the spectrum of the pure Tween-20 also provided for reference purposes. IR absorbance bands characteristic of organic moieties such as the OH stretch (3400-3200 cm^{-1}), aliphatic C-H stretch (3000-2900 cm^{-1}), and fingerprint region C-O stretch (1100 cm^{-1}) are present in the spectrum of the Tween-20 coated MMFNPs, albeit with significantly reduced intensity relative to the spectrum of the unadulterated Tween-20. This indicates successful incorporation of the Tween-20 onto the surface of the MMFNPs.

Tween-20 (a nonionic surfactant) coating shifts ferrite NP ζ potentials toward slightly negative values, typically around -20 mV or less; however, this is only the case if the measured value is dominated by adsorbed Tween rather than the bare MMFNP surface[63]. Tween-20 adsorbs on MFe_2O_4 NP surfaces through hydrophobic and hydrogen-bond interactions, but carries no net charge; thus, it tends to screen or compress the native surface charge, rather than introduce a strong new one. Table 3 reveals that the students measured the surface zeta potential of $NiFe_2O_4$ to be -14 mV, while for the other two systems, the numerical values of the ζ potential were higher than expected (*ca.* -30 mV for $MnFe_2O_4$ and -27 mV for $CoFe_2O_4$). Given the preparation history of our samples in strongly basic media, the as-prepared ferrite NPs are expected to show strongly negative ζ potential values, owing to the presence of surface-adsorbed OH^-. If the post-synthesis washing steps are not comprehensive, this effect is amplified. Retention of this negative charge on the ferrite NPs despite the nominal presence of a Tween-20 surface coating is indicative of incomplete surface coverage by the surfactant. The presence of metal hydroxyl ($M-OH$) species on the surface of the MMFNPs, which subsequently deprotonate to form $M-O^-$ species, may also lead to highly negative surface ζ-potential values, especially if meticulous washing is not carried out, leading to base contamination of the dried MMFNPs. These nuances were explained to the students to account for the discrepancy between the literature and the measured values.

* The students started a new experiment unrelated to this manuscript during week 6.

View Article Online
DOI: 10.1039/D6SU00221H

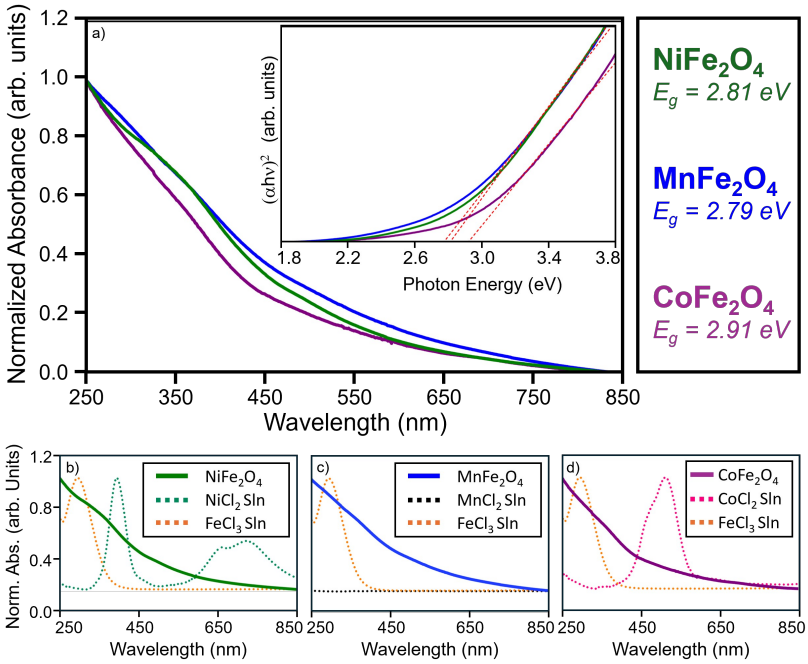

Fig. 2 (a) Normalized absorbance of MMFNPs with the inset showing the $(ahv)^2$ Tauc plots and linear fits. (b-d) Normalized absorbance of MMFNPs compared to those of the aqueous precursors. In (c), the absorbance of the $MnCl_2$ solution is not normalized, as minimal absorbance was detected across the range.

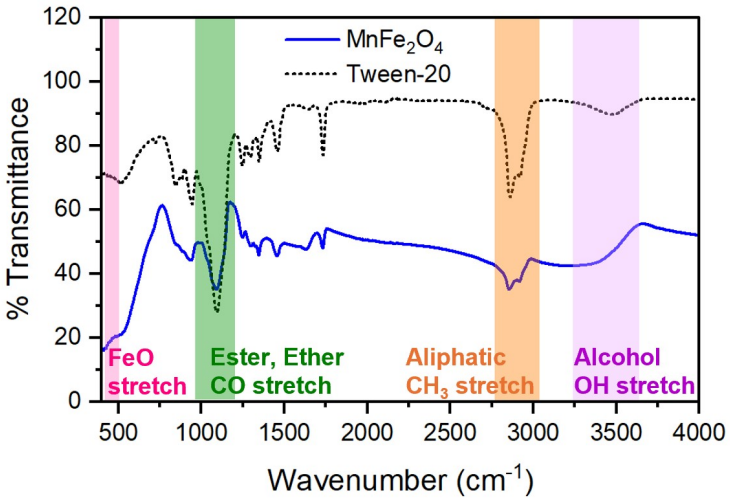

Fig. 3 FTIR spectra of Tween-20 and the Tween-coated $MnFe_2O_4$ nanoparticles. The highlighted areas indicate pedagogically relevant IR bands for the two samples.

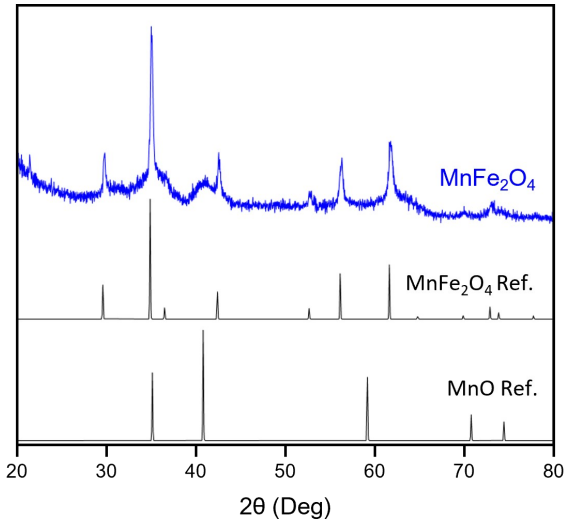

Fig. 4 Experimental powder diffraction pattern for the $MnFe_2O_4$ nanoparticles, as well as reference patterns for $MnFe_2O_4$ (COD 1528316) and MnO (COD 1010393) 'matchstick plots'.[64,65]

3.4 Phase properties: Powder X-ray diffraction (PXRD).

The identification of the synthesized nanomaterial phase is critical to subsequent functional testing[66], owing to the phase-dependence of physicochemical, optical, and electronic properties. However, the sheer cost and difficulty of acquiring and running powerful and reliable powder or single crystal diffraction instrumentation suites prevented many UG lab courses from including this vital technique within their syllabi in the past. While this has changed somewhat with the availability of bench-top systems, manufacturers still require subscriptions to proprietary data analysis software and structural databases, such as the International Center for Diffraction Data (ICDD) database. It is our contention that sample preparation as well as analysis and phase matching of the collected data is more significant for UG researchers than hands on data collection, when it comes to PXRD. Accordingly, we used the following strategies to get around the aforementioned barriers:

1. Collaboration: EC, one of the authors, is the departmental

View Article Online
DOI: 10.1039/D6SU00221H

expert staff crystallographer, and used his discretionary machine time for data collection. We also borrowed the zero-background sample holders from EC for students to practice sample deposition on. The evenness of the deposition was gauged by EC and his feedback was relayed to the students.

2. Community databases: An excellent alternative to paid databases is the free to access Crystallography Open Database (COD), which allows prospective crystallographers to browse hundreds of thousands of small molecule and material crystal structures in the form of crystallographic information files (*.cif*). While not as extensive as, for example, the ICDD database, obtaining structural data for the analysis of commonly synthesized materials with limited options for phase identity (such as the MMFNPs explored here) is easily achieved using the COD[46–54].

3. Freeware or CSU-licenced software: Finally, easily downloadable structural data allows the phase identification to be completed with software ranging from Microsoft Excel® or OriginLab® to specialized crystallography tools like Mercury® or CrystalDiffract® (used here). Many of these are either freeware or were procured using a departmental licence.

In the third week, students received the experimental powder diffractograms recorded for their assigned MMFNP sample. In addition, the students were trained on obtaining appropriate data (in *.cif* format) from COD for potential phase matches. This tutorial also exposed students to vital aspects of phase identification, such as Bragg peak matching, relative intensities, and peak width determination. The students were then assigned to make matchstick-like plots for their individual experimental data, as well as possible primary phase and impurity phase matches, to be included in their final communication-style report. An example of this is shown in Figure 4 for the $MnFe_2O_4$ nanoparticles. Bragg peaks corresponding to the (220), (311), (400) (511), and (440) indices of $MnFe_2O_4$ are observed at 30, 34, 42, 56, and 61 on the 2θ axis, and match in relative intensity to the provided reference, confirming that the spinel jacobsite was obtained as the primary phase[67]. However, a notable impurity at $2\theta = 40$ was observed; this was matched to the (200) index of MnO[68]. The obtained diffraction patterns for all MMFNPs synthesized by the students are available in the Supporting Information with associated references; we note that the nominal $NiFe_2O_4$ NPs failed to yield a strong diffraction pattern, indicating a lower degree of crystallinity in that particular sample; this is addressed in some detail in the ESI. The students responsible for this particular synthesis were expected to make a note of this in their communication.

3.5 Size and morphological properties: SEM, DLS and PXRD.

Students used these three aforementioned techniques to characterize the size, morphology, and phase of their prepared ferrite NPs. It is important to note that DLS, SEM and PXRD can individually provide us with information about NP sizes - however, the sizes determined from these three routes are not expected to be identical. Dynamic light scattering (DLS) reports an intensity-weighted hydrodynamic diameter in dispersion that includes the inorganic core plus any solvation layer and surface adsorbates, so it usually gives larger apparent sizes and is very sensitive to aggregates and polydispersity. Scanning electron microscopy (SEM) provides direct images of dried particles, giving a number-based physical core size and shape, but preparation (drying, aggregation, coating, limited statistics) can bias the measured diameter compared with the true dispersed state. Powder X-ray diffraction (PXRD) with Scherrer equation yields a volume-averaged crystallite size derived from peak broadening, which reflects coherent crystalline domains rather than whole particles, and therefore underestimates size when particles are polycrystalline or aggregated and ignores amorphous particles.

Figure 5 shows SEM micrographs (with and without colourization) of the $MnFe_2O_4$/Tween-20 NPs. The expected grape-like clusters of quasi-spherical NPs are seen, representative of co-precipitated NPs with moderate size control. Particles show a slightly faceted or 'stone-like' appearance due to crystalline facets[69]. Soft agglomerates rather than isolated primary particles are seen, because of magnetic and van der Waals interactions; individual grains appear to be embedded in larger micron-scale aggregates[70].

The determination of crystallite sizes from the Scherrer equation was also part of the data processing skills imparted to the students. The Scherrer plot and the obtained size average of $MnFe_2O_4$ crystallites has been represented in Figure 6(a). Fig 6(b) shows the bimodal size distribution profile of the Tween-20-capped $MnFe_2O_4$ NPs in water as obtained DLS. A minor population (< 10 nm in size) probably represent $MnFe_2O_4$ seeds or ultrasmall NPs whose growth may have been attenuated by the surfactant; the the major population with average NP sizes in the 100-150 nm range are likely the fully-grown counterparts of the smaller ferrite NPs.

From Figures 5 and 6, we see that the following general trend for oxide NPs, *viz,*; Scherrer sizes $<$ SEM core sizes $<$ DLS hydrodynamic diameters; holds true for nearly all the samples. The students were expected to understand that these three protocols for the size determination of ferrite NPs are complementary rather than interchangeable.

Table 3 Surface zeta potential and average size of student-synthesized MMFNPs.

Sample	ζ potential (mV)	Scherrer size (nm)	SEM size (nm)	DLS size (nm)
$NiFe_2O_4$	-14.1±2.8	amorphous	98±29	4.6±2.3 134±62
$MnFe_2O_4$	-29.2±2	30.8	118±38	5.4±2.1 129±58
$CoFe_2O_4$	-27.4±7	23.7	97±26	30±14 190±30

View Article Online
DOI: 10.1039/D6SU00221H

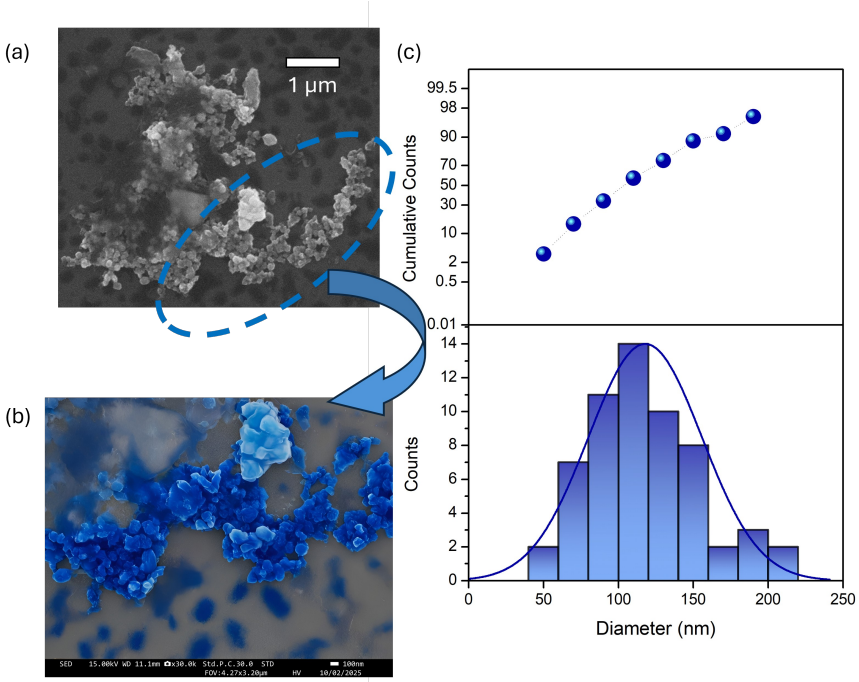

Fig. 5 (a and b) SEM secondary electrons images of the same student sample of $MnFe_2O_4$-Tween-20 NPs at lower and higher magnifications, respectively. The lower magnification image is presented as-is; the 'zoomed-in' image is colourized by the student through the use of AI *(https://imagecolorizer.com/colorize)*; (c) particle size frequency distribution profile and probability from manual measuring of at least 100 spherical $MnFe_2O_4$ NPs from the images.

3.6 Sustainability and catalytic application: Fenton-type degradation of methylene blue

Beyond the utilization of green chemical techniques for synthesis and the focus on nontoxic and environmentally friendly precursors, the simulation of nanoparticle-catalyzed wastewater remediation is an ideal way to help students connect core ideas of sustainability to nanochemistry.[71] The removal and management of contaminants in wastewater is a vital yet understated part of mitigating greater environmental concerns. Ferrite NPs are ideal for this purpose: $CoFe_2O_4$, for instance, has been known to catalyze the decomposition of H_2O_2 as effectively as Pt, Pd or silver oxide catalysts[72]. In our study, we chose methylene blue, a complex, non-biodegradable conjugated dye, to act as a typical representative of common organic pollutants. In particular, ingesting water contaminated with methylene blue (and other similar pollutants) has been linked to cases of respiratory distress, neurotoxicity, blindness, digestive and abdominal disorders, alongside physical discomfort upon prolonged dermal contact[73]. The MMFNPs from this project are effecitve, safe, and environmentally friendly catalysts, with the added bonus of magnetic activity allowing for easy catalyst recovery and recycling.

Our example reaction utilizes a class of reactions broadly termed 'Fenton chemistry', in which refractory organics in an aqueous matrix (such as a solution of methylene blue in water) is broken down into smaller, colourless fragments, thereby effectively decolurizing it[74]. This is achieved by adding the MMFNPs to an aqueous solution of the dye and H_2O_2 under UV light irradiation. Fenton reactions use the classic Fe(II)/H_2O_2 system for catalysis, while 'Fenton-type' (or Fenton-like) reactions generalize this chemistry to other oxidants, metals, and conditions, as we have done here with the use of MMFNPs.[75] This process has three distinct advantages for pedagogical application:

1. H_2O_2 breaks down into water, making it a benign 'green' oxidant;

2. The kinetics of the MMFNP catalyzed degradation are extremely fast, allowing for multiple catalytic cycles (reaction-recovery-reaction...) to be completed in one lab period; and,

3. The progress of the reaction can be estimated through visual inspection (the colour of the dye fades as the reaction progresses) and easily quantifiable using simple optical spectroscopy.

A sample one-run procedure as followed by the students is available in the ESI. It must be noted that prior to the addition of the MMFNPs, the pH was adjusted to 10-11 by dropwise addition of NaOH; peroxide decompositions are generally studied in alkaline media where H_2O_2 is intrinsically unstable because of base catalysis by OH^-[72]. Students were encouraged to consider the consequence of performing the reaction at an alkaline pH, mainly the inhibition caused by the formation and precipitation of competing $Fe(OH)_3$ species[76]. The progress of the degradation reaction as performed by the students using each respective ferrite species are shown in Figure 7(a-c). The observed decrease of the main methylene blue absorption transition (*ca.* 660 nm) over time reveals that all three of the student-synthesized MMFNPs successfully catalyzed the peroxide-mediated decomposition of

View Article Online
DOI: 10.1039/D6SU00221H

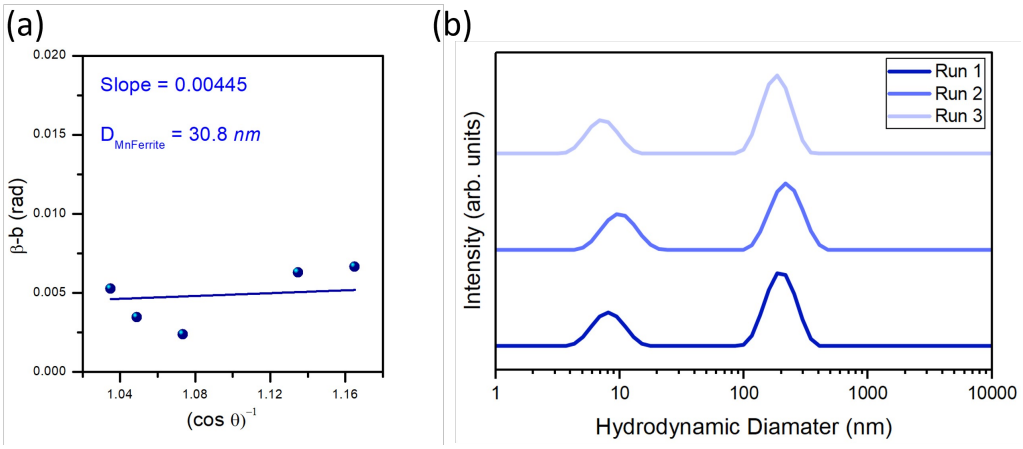

Fig. 6 (a) Scherrer plot of the $MnFe_2O_4$ NPs for obtaining crystallite size from the diffractogram; (b) DLS size distribution profile for an aqueous dispersion of $MnFe_2O_4$/Tween-20 NPs showing a bimodal size distribution.

methylene blue over a sixty-minute span. Students were then reminded of the Beer-Lambert law, relating the absorbance at each time point to the concentration of methylene blue in solution at that instant. This relationship allowed them to plot the natural log of the absorbance at 660 nm against the reaction time, with the slope of the resulting line corresponding to the pseudo-first-order rate constant, as shown in Figure 7d. The k_{pseudo} (as determined from least-square regression) varied from 0.073 min^{-1} ($NiFe_2O_4$, fastest) to 0.043 min^{-1} ($CoFe_2O_4$) and 0.034 min^{-1} ($MnFe_2O_4$, slowest). The % degradation of methylene blue at time t was calculated using the following formula:

$$\%\, degradation = \frac{(A_t - A_0)}{A_0} \times 100 \quad (3)$$

where A_0 and A_t represent the absorbance (at λ_{max}) at the beginning of the reaction and at time t, respectively.

After *ca.* 60 mins, all MMFNPs displayed more than 80% degradation efficiency, which is broadly in agreement with the many research-focused studies of methylene blue remediation[74,77]. The students also observed that the identity of the transition metal 'dopant' (*i.e.* Mn, Ni, or Co) appeared to affect catalytic efficiency of the spinel NP. Here, students were cautioned not to attribute causation to a correlation, as catalytic efficiency can depend on particle size, surface chemistry, structure, and other factors, which may obfuscate impacts on catalytic activity that could be the result of compositional differences[78]. Furthermore, the amorphous nature of the $NiFe_2O_4$ precludes any 'apples-to-apples' comparison here.

After the first reaction was completed, the students used a standard laboratory magnetic stir bar to successfully reclaim the majority of their MMFNP catalyst. The degradation process was then repeated twice more, for a total of three catalytic cycles utilizing the same catalyst. The degradation efficiency for three replicate degradation reactions using $CoFe_2O_4$ nanoparticles as the catalyst is shown in Figure 8. After sixty minutes, the efficiencies for each replicate remained above 80%, demonstrating the reusability of the MMFNPs. Recoverability and recyclability of the MMFNP catalysts are major reasons why ferrite catalysts are considered sustainable, and students were exposed firsthand to the observable benefit of a high-performing reusable catalyst.

3.7 LLM incorporation within the workflow

Incorporating a Large Language Model (LLM) (here, Google Gemini) into this nanochemistry mini-project transforms the experience into a dynamic, AI-augmented CURE. By integrating AI into every segment, from MMFNP synthesis, to characterization, and to application, students develop critical digital literacy and "human-in-the-loop" verification skills essential for modern research[41].

Below, we briefly describe the role played by LLM in different segments of the CURE:

1. **Synthesis:** During the co-precipitation synthesis, the LLM serves as a predictive tool. Before synthesis, students use Gemini to hypothesize the effect of the base addition rate (*e.g.*, 1 mL every 10 s) and pH (aiming for 10-11) on nanoparticle size and polydispersity. The students also used LLM to figure out the reason behind the low crystallinity of $NiFe_2O_4$ versus the other ferrites, despite identical synthesis conditions.

2. **LLM-assisted preliminary data interpretation:** Students use Google Gemini to navigate the preliminary interpretation of the data collected from the characterization techniques. For UV-Vis and IR data, students use the LLM to assist in identifying chemically relevant peaks common to Tween-20 and the Tween-20 capped MMFNPs. In the PXRD segment, students prompt the LLM to explain the structural differences between probable phases such as MFe_2O_4 and $M^{II}O$ (M = Ni,Co,Mn). LLM also points them towards the correct *.cif* files for the relevant phases, harvested from sources such as the Open Crystallographic Database, and introduces them to the effective use of freeware for unit cell visualization from *.cif* files after the initial hands-on training conducted in person. LLMs also come in handy during the interpretation of DLS results, especially the ζ-potential values. Finally, while using FiJi for SEM image analysis, students consult the

View Article Online
DOI: 10.1039/D6SU00221H

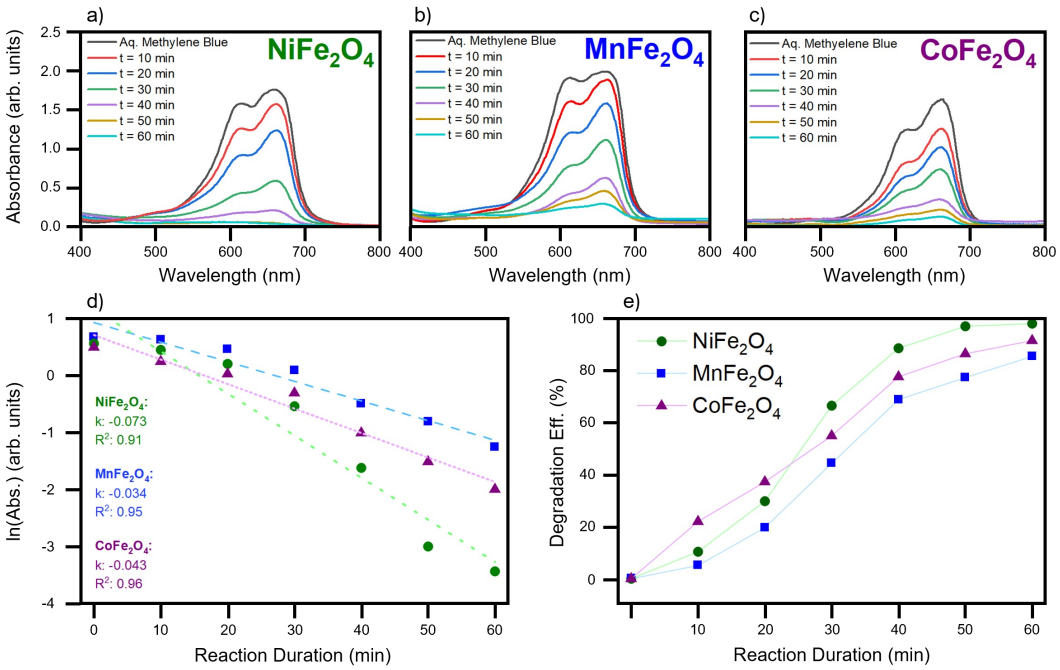

Fig. 7 (a-c) Optical spectra of methylene blue throughout the Fenton-type degradation reactions catalyzed with (a) $NiFe_2O_4$, (b) $MnFe_2O_4$, and (c) $CoFe_2O_4$ nanoparticles, respectively. (d) Plot of $lnA_{(\lambda=660nm)}$ as a function of reaction time (A = recorded absorbance). The slope of the line of best fit gives the pseudo-first-order reaction rate. (e) Degradation efficiency as a function of reaction time for the Fenton-type degradation of methylene blue catalyzed by the MMFNPs.

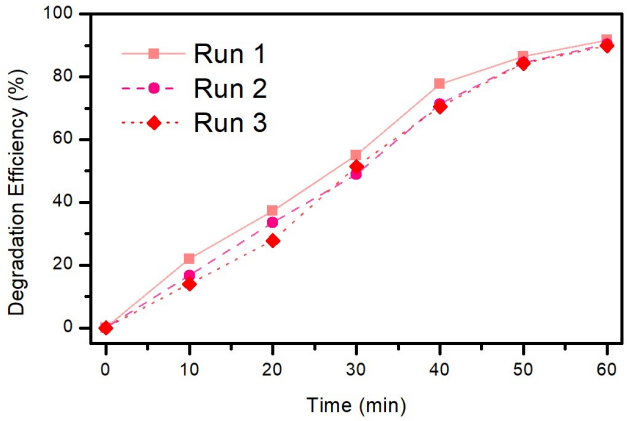

Fig. 8 Degradation efficiency of as-prepared and recycled $CoFe_2O_4$ NPs in degrading methylene blue.

LLM for advanced plugins or macros to automate the measurement of at least 100 MMFNP diameters for statistical plotting[79]. AI-enabled digital colourization of the electron micrographs also proved to be a popular and enjoyable student activity.

3. **LLM for sustainable process design:** In the methylene blue degradation application, the LLM bridges the gap between the lab and global sustainability goals. Students prompt Gemini to model the oxidative degradation of methylene blue in the presence of H_2O_2, UV light, and MMFNPs, troubleshooting issues such as initial sluggishness. LLM may also be used to propose modifications to the experiment that would further reduce chemical waste or enhance the 'greenness' of the catalytic cycle.

4. **LLM usage log maintenance for verification:** To ensure that the use of the LLM remains a tool for critical inquiry rather than a shortcut for answers, students in this CURE were encouraged to maintain and periodically validate a verification log[80]. This log serves as a structured record of their interactions with Google Gemini, specifically documenting how they validated LLM-generated claims against empirical data and primary literature. A recommended structure for the verification log includes the following components: (i) prompt and context; (ii) output summary; and (iii) validation (by the students themselves, or the GTA).

   A sample validation log may be found in the ESI.

Conclusions

In 2026, for a record fifth consecutive time, Colorado State University has earned a Platinum rating from the Association for the Advancement of Sustainability in Higher Education, reaffirming its reputation as an innovative leader in sustainability[81]. Therefore, involving aspects of sustainability in upper-year chemistry courses is timely and appropriate. In this paper, we describe the implementation of a CURE-type experiment involving the synthesis, characterization, and evaluation of the catalytic potential of environmentally friendly transition metal ferrite nanoparticles (MFe_2O_4, M = Ni, Mn, Co) coated with a non-toxic capping ligand. The experiment serves as an introduction to

View Article Online
DOI: 10.1039/D6SU00221H

the nanochemistry-specific laboratory course offered at Colorado State University. In particular, this experiment was designed to lay the groundwork for successful course completion by introducing key laboratory concepts in the realm of nanoscience that was required throughout the rest of the semester. Comprehensive and multidisciplinary inquiry-guided experiments such as this one, conducted over multiple laboratory sessions, provide the opportunity to simulate a research environment, reinforcing data analysis, scientific writing, and laboratory skills through a series of linked experiences.

LLMs, we have been told, are here to stay, and as they grow more powerful and nuanced, and are widely used by students, we can no longer isolate our pedagogical strategies from their influence. This study is our inaugural attempt to integrate LLMs within our sustainable nanochemistry CURE. From received feedback, we find that LLMs significantly enrich the student inquiry process, provided it is used ethically and with concomitant validation. The implementation of LLMs facilitated several key educational and scientific objectives. LLMs served as an iterative sounding board, allowing students to refine their hypotheses regarding NP surface chemistry and the kinetics of radical generation. Students leveraged LLM to troubleshoot characterization and kinetic data analysis. LLMs also maintained focus on recyclable catalysts, emphasized the principles of Green Chemistry, and provided the necessary context for follow-up questions such as process scale-up and life-cycle analysis of magnetic nanoparticles.

Ultimately, this hybrid pedagogical approach does more than just modernize the laboratory experience; it equips future chemists with the AI fluency required to navigate an increasingly digital research landscape. While the ferrite NPs provide a robust physical platform for studying advanced oxidation processes, the LLM provides the cognitive scaffolding necessary for high-level synthesis and critical inquiry. We expect future studies to explore the scalability of this framework across other sub-disciplines of chemical education.

Author contributions

Conceptualization – AB; data curation – AB, JED, EC; formal analysis – AB, JED, EC; funding acquisition – AB; investigation – JED, EC; methodology – AB, EC; project administration – AB; supervision – AB; visualization – AB, EC, JED; writing (original draft) – AB, JED; writing (review & editing) – all authors.

Conflicts of interest

There are no conflicts to declare.

Data availability

The data supporting this article have been included as part of the Supplementary Information, as well as in the figures and tables of the main article. Raw data generated by the students will be anonymized and produced upon request.

Acknowledgements

We acknowledge the help we received from Analytical Resources Core (ARC; RRID: SCR_021758) for the duration of this experiment. Figure 1 was created with BioRender.

Notes and references

1 A. L. Porter and I. Rafols, *Scientometrics*, 2009, **81**, 719–745.
2 J. Ren, F. Wang and M. Li, *Scientometrics*, 2023, **128**, 4383–4419.
3 T. Fuhrmann-Lieker, *Nanoethics*, 2024, **18**, 15.
4 A. Banerjee, G. E. Bertolesi, C.-C. Ling, B. Blasiak, A. Purchase, O. Calderon, B. Tomanek and S. Trudel, *ACS Appl. Mater. Interfaces*, 2019, **11**, 13069–13078.
5 A. Banerjee and R. W. Scott, *Green Chem.*, 2015, **17**, 1597–1604.
6 J. Hulla, S. Sahu and A. Hayes, *Hum Exp Toxicol*, 2015, **34**, 1318–1321.
7 Q. Zhang, E. Uchaker, S. L. Candelaria and G. Cao, *Chem. Soc. Rev.*, 2013, **42**, 3127–3171.
8 A. Tripathi and J. Bonilla-Cruz, *ACS Appl. Nano Mater.*, 2023, **6**, 5042–5074.
9 W. J. Stark, P. R. Stoessel, W. Wohlleben and A. Hafner, *Chem. Soc. Rev.*, 2015, **44**, 5793–5805.
10 H. M. Gramling, M. E. Kiziroglou and E. M. Yeatman, *Nanoelectronics*, John Wiley & Sons, Ltd, 2017, pp. 501–526.
11 M. M. Khin, A. S. Nair, V. J. Babu, R. Murugan and S. Ramakrishna, *Energy Environ. Sci.*, 2012, **5**, 8075–8109.
12 J. A. Jackman, D.-J. Cho, J. Lee, J. M. Chen, F. Besenbacher, D. A. Bonnell, M. C. Hersam, P. S. Weiss and N.-J. Cho, *ACS Nano*, 2016, **10**, 5595–5599.
13 M. Pagliaro, *Chem. Eur. J.*, 2015, **21**, 11931–11936.
14 N. Chopra and R. G. Reddy, *JOM*, 2012, **64**, 1127–1129.
15 T. Schwantes, D. Medina, B. Morgan and A. Banerjee, *RSC Sustain.*, 2025, **3**, 3437–3447.
16 D. Zuo, G. Kim and D. Jones, *J. Nano Educ.*, 2019, **11**, 1–8.
17 M. L. Landry, T. E. Morrell, T. K. Karagounis, C.-H. Hsia and C.-Y. Wang, *J. Chem. Educ.*, 2014, **91**, 274–279.
18 A. J. Buchanan and G. R. Fisher, *LSE*, 2022, **21**, ar83.
19 J. J. Provost, *J. Chem. Educ.*, 2022, **99**, 3842–3848.
20 F. M. Watts and J.-M. G. Rodriguez, *J. Chem. Educ.*, 2023, **100**, 3261–3275.
21 G. Bangera and S. E. Brownell, *CBE Life Sci Educ*, 2014, **13**, 602–606.
22 J. G. D'Angelo, *J. Chem. Educ.*, 2023, **100**, 2904–2916.
23 O. Love, M. Heying, P. R. Steed and S. A. Wasileski, *J. Chem. Educ.*, 2024, **101**, 2757–2764.
24 D. Gupta, A. Boora, A. Thakur and T. K. Gupta, *Environ. Res.*, 2023, **231**, 116316.
25 H. Duan, D. Wang and Y. Li, *Chem. Soc. Rev.*, 2015, **44**, 5778–5792.
26 M. Naghdi, M. Taheran, S. K. Brar, M. Verma, R. Y. Surampalli and J. R. Valero, *Beilstein J. Nanotechnol.*, 2015, **6**, 2354–2376.
27 N. Hasan, M. Muthu, O. Hakami and J. Gopal, *Energies*, 2025, **18**, 523.
28 N. Ajinkya, X. Yu, P. Kaithal, H. Luo, P. Somani and S. Ramakrishna, *Materials*, 2020, **13**, 4644.
29 W. Ling, M. Wang, C. Xiong, D. Xie, Q. Chen, X. Chu, X. Qiu,

View Article Online
DOI: 10.1039/D6SU00221H

Y. Li and X. Xiao, *J. Mater. Res.*, 2019, **34**, 1828–1844.
30 S. J. Salih and W. M. Mahmood, *Heliyon*, 2023, **9**, 1–25.
31 A.-G. Niculescu, C. Chircov and A. M. Grumezescu, *Methods*, 2022, **199**, 16–27.
32 A. Banerjee, B. Blasiak, E. Pasquier, B. Tomanek and S. Trudel, *RSC Adv.*, 2017, 38125–38134.
33 P. A. Vinosha, B. Xavier, D. Anceila and S. J. Das, *Optik*, 2018, **157**, 441–448.
34 M. Ebrahimi, R. Raeisi Shahraki, S. A. Seyyed Ebrahimi and S. M. Masoudpanah, *J Supercond Nov Magn*, 2014, **27**, 1587–1592.
35 Q. Guo, J. Zhen, F. Wu, Y. He and C. Qiao, *J. Educ. Comput. Res.*, 2025, **63**, 372–405.
36 M. Lissack and B. Meagher, *SSRN*, 2024, **4949829**, 1–18.
37 S. Kim, Y. Jung and J. Schrier, *J. Am. Chem. Soc.*, 2024, **146**, 19654–19659.
38 R. M. Perez, M. Shimogawa, Y. Chang, X. Li, H. A. T. Phan, J. G. Marmorstein, E. S. Yanagawa and E. J. Petersson, *Comput. Educ. Artif. Intell.*, 2026, **10**, 100546.
39 K.-H. Yim and M. Y. Lui, *J. Chem. Educ.(ASAP article)*, 2026, **doi:10.1021/acs.jchemed.5c01311**,.
40 P. M. Hare, *J. Chem. Educ.*, 2024, **101**, 3869–3874.
41 A. E. Maughan, E. S. Toberer and A. Zevalkink, *Chem. Mater.*, 2025, **37**, 2389–2394.
42 Y. Li, L. Tolosa, F. R. Echeverria and R. Marquez, *J. Chem. Educ.*, 2026, **103**, 1135–1144.
43 J. Kim, *J. Chem. Educ.*, 2025, **102**, 3058–3064.
44 Y.-F. Gao, D. Meng, X.-Y. Li, S.-H. Wang, J.-X. Chen, R.-Y. Cao, Y.-T. Zhai, J.-E. Hu, Q.-L. Bai, Z.-P. Zhang, Y.-Y. Li, K. Li and S.-Q. Zang, *J. Chem. Educ.*, 2025, **102**, 2436–2442.
45 *CrystalMaker Software Ltd*, `www.crystalmaker.com`, 2025.
46 A. Vaitkus, A. Merkys, T. Sander, M. Quirós, P. A. Thiessen, E. E. Bolton and S. Gražulis, *J. Cheminform.*, 2023, **15**, 123.
47 A. Merkys, A. Vaitkus, A. Grybauskas, A. Konovalovas, M. Quirós and S. Gražulis, *J. Cheminform.*, 2023, **15**, 25.
48 A. Vaitkus, A. Merkys and S. Gražulis, *J. Appl. Crystallogr.*, 2021, **54**, 661–672.
49 M. Quirós, S. Gražulis, S. Girdzijauskaitė, A. Merkys and A. Vaitkus, *J. Cheminform.*, 2018, **10**, 23.
50 A. Merkys, A. Vaitkus, J. Butkus, M. Okulič-Kazarinas, V. Kairys and S. Gražulis, *J. Appl. Crystallogr.*, 2016, **49**, 292–301.
51 S. Gražulis, A. Merkys, A. Vaitkus and M. Okulič-Kazarinas, *J. Appl. Crystallogr.*, 2015, **48**, 85–91.
52 S. Gražulis, A. Daškevič, A. Merkys, D. Chateigner, L. Lutterotti, M. Quirós, N. R. Serebryanaya, P. Moeck, R. T. Downs and A. Le Bail, *Nucleic Acids Res.*, 2012, **40**, D420–D427.
53 S. Gražulis, D. Chateigner, R. T. Downs, A. F. T. Yokochi, M. Quirós, L. Lutterotti, E. Manakova, J. Butkus, P. Moeck and A. Le Bail, *J. Appl. Crystallogr.*, 2009, **42**, 726–729.
54 R. T. Downs and M. Hall-Wallace, *Am. Mineral.*, 2003, **88**, 247–250.
55 C. F. Macrae, I. Sovago, S. J. Cottrell, P. T. A. Galek, P. McCabe, E. Pidcock, M. Platings, G. P. Shields, J. S. Stevens, M. Towler and P. A. Wood, *J. Appl. Crystallogr.*, 2020, **53**, 226–235.
56 J. Sherin, T. Bessy, S. Asha, C. V. Kumar, D. Huessien, M. Bindhu, R. A. Rasheed and K. M. Alarjani, *Environ. Res.*, 2022, **208**, 112687.
57 M. Gurumoorthy, G. Palani, H. Trilaksanna and M. Kumar, *Anal. Chem. Lett.*, 2024, **14**, 848–861.
58 S.-K. Tong, P.-W. Chi, S.-H. Kung and D.-H. Wei, *Sci Rep*, 2018, **8**, 1338.
59 K. V. Chandekar, M. Shkir and S. AlFaify, *Mater. Sci. and Engg. B*, 2020, **259**, 114603.
60 N. Bhalla, S. Taneja, P. Thakur, P. K. Sharma, D. Mariotti, C. Maddi, O. Ivanova, D. Petrov, A. Sukhachev, I. S. Edelman and A. Thakur, *Nano Lett.*, 2021, **21**, 9780–9788.
61 J. Klein, L. Kampermann, B. Mockenhaupt, M. Behrens, J. Strunk and G. Bacher, *Adv. Func. Mater.*, 2023, **33**, 2304523.
62 A. Banerjee, R. Theron and R. W. Scott, *ChemSusChem*, 2012, **5**, 109–116.
63 H. Cortés, H. Hernández-Parra, S. A. Bernal-Chávez, M. L. D. Prado-Audelo, I. H. Caballero-Florán, F. V. Borbolla-Jiménez, M. González-Torres, J. J. Magaña and G. Leyva-Gómez, *Materials*, 2021, **14**, 3197.
64 B. Antic, A. Kremenovic and A. Stioljkovic, M.and Nikolic, *J. Phys. Chem. B*, 2004, **108**, 12646–12651.
65 C. Fontant, *Gazzetta Chimica Italiana*, 1926, **56**, 396–397.
66 D. R. Baer, M. H. Engelhard, G. E. Johnson, J. Laskin, J. Lai, K. Mueller, P. Munusamy, S. Thevuthasan, H. Wang, N. Washton and D. Moon, *J. Vac. Sci. Technol. A*, 2013, **31**, 050820.
67 M. Bellusci, S. Canepari, G. Ennas, A. L. Barbera, F. Padella, A. Santini, A. Scano, L. Seralessandri and F. Varsano, *J. Am. Ceram. Soc.*, 2007, **90**, 3977–3983.
68 X.-F. Shen, Y.-S. Ding, J. C. Hanson, M. Aindow and S. L. Suib, *J. Am. Chem. Soc.*, 2006, **128**, 4570–4571.
69 S. Sugi, S. Radhika and C. Padma, *Mater. Chem. Phys.*, 2022, **292**, 126799.
70 S. Schyck, N. Rajendra Madam and L. Rossi, *Soft Matter*, 2025, **21**, 3197–3206.
71 Y. Chen, L. Cai, J. Gong and H. Lai, *J. Chem. Educ.*, 2023, **100**, 1597–1602.
72 P. Lahiri and S. K. Sengupta, *Can. J. Chem.*, 1991, **69**, 33–36.
73 M. Bužga, E. Machytka, E. Dvořáčková, Z. Švagera, D. Stejskal, J. Máca and J. Král, *Toxicol. Res.*, 2022, **11**, 711–717.
74 M. Golshan, B. Kakavandi, R. Pelalak and Y. Bao, *J. Water Process Eng.*, 2025, **75**, 107873.
75 S. A. Walling, W. Um, C. L. Corkhill and N. C. Hyatt, *npj Mater. Degrad.*, 2021, **5**, 50.
76 M. L. Kremer, *J. Phys. Chem. A*, 2003, **107**, 1734–1741.
77 A. Kalam, A. G. Al-Sehemi, M. Assiri, G. Du, T. Ahmad, I. Ahmad and M. Pannipara, *Results Phys.*, 2018, **8**, 1046–1053.
78 A. S. Albuquerque, M. V. Tolentino, J. D. Ardisson, F. C. Moura, R. de Mendonça and W. A. Macedo, *Ceram. Int.*, 2012, **38**, 2225–2231.

View Article Online
DOI: 10.1039/D6SU00221H

79 K. M. Aviles and B. J. Lear, *ACS Nanosci. Au*, 2025, **5**, 117–127.

80 S. S. Subasinghe, S. G. Gersib and N. P. Mankad, *J. Chem. Educ.*, 2025, **102**, 1563–1571.

81 Joe Giordano, Colorado State University: SOURCE, *CSU is on top of the world in sustainability*, URL: `https://source.colostate.edu/csu-is-on-top-of-the-world-in-sustainability/`, 2026.

82 P. Scherrer, *Nachr. Ges. Wiss. Gött., Math.-Phys. Kl.*, 1918, **1918**, 98–100.

View Article Online
DOI: 10.1039/D6SU00221H

Data availability

The data supporting this article have been included as part of the Supplementary Information, as well as in the figures and tables of the main article. Raw data generated by the students will be anonymized and produced upon request.